## Supplemental Figures

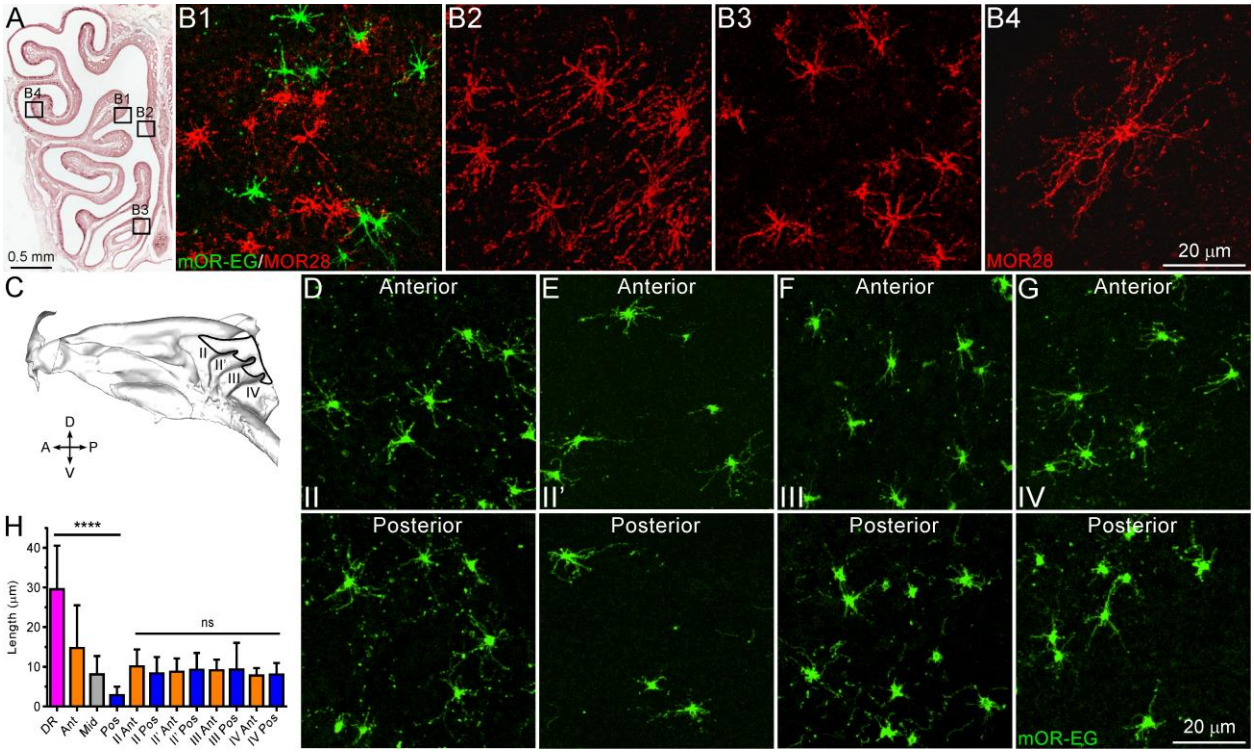


**Figure S1, related to Figure 1. The Ventral Zone, as well as the Dorsal Zone along the Endoturbinates, Do Not Exhibit Systematic Regional Differences in Cilia Length.** In whole mount epithelia from mOR-EG-IRES-gapEGFP mice, mOR-EG cells were examined via the endogenous GFP signal (green) and MOR28 cells via an antibody against the MOR28 receptor (red). (**A** and **B**) A coronal section of the nose (**A**) indicates the approximate regions in which confocal images were taken (black boxes): endoturbinate II (**B1**), ventral septum (**B2**), endoturbinate IV (**B3**), and ectoturbinate 2 (**B4**). Scale bar in (B4) applies to (B1-B4). See (C) for a sagittal view of the medial surface of the endoturbinates. We noticed that MOR28 cells in the ectoturbinates have slightly longer cilia than those along the septum and endoturbinates. This difference is likely attributed to variations in multiple factors including mucosal environment and cell dynamics among different regions. For simplicity, we refer to regions with mOR-EG and MOR28 positive cells as the dorsal and ventral zones, respectively. Note that mOR-EG and MOR28 cells are observed simultaneously in narrow transitional regions (B1), which presumably represent the intermediate zone between the dorsal and ventral zones. (**C-G**) Schematic of the medial surface of endoturbinates II-IV (**C**): A = anterior; D = dorsal; P = posterior; V = ventral. Images were taken from the anterior and posterior regions of turbinates II (**D**), II' (**E**), III (**F**), and IV (**G**). Scale bar in (G) applies to (D-G). (**H**) The bar graph shows quantification of cilia length (mean ± SD). II – Ant: 10.1 ± 4.2 μm, n = 53 cilia; Pos: 8.3 ± 4.1 μm, n = 65 cilia; II' – Ant: 8.7 ± 3.4 μm, n = 61 cilia; Pos: 9.2 ± 4.2 μm, n = 55 cilia; III – Ant: 9.1 ± 2.8 μm, n = 66 cilia; Pos: 9.3 ± 6.7 μm, n = 57 cilia; IV – Ant: 7.8 ± 1.9 μm, n = 54 cilia; Pos: 8.0 ± 2.9 μm, n = 64 cilia; one-way ANOVA, $F = 111.4$; Tukey's multiple comparisons test, **** $p < 0.0001$, ns – not significant. See Figure 1C for quantification from the septum.

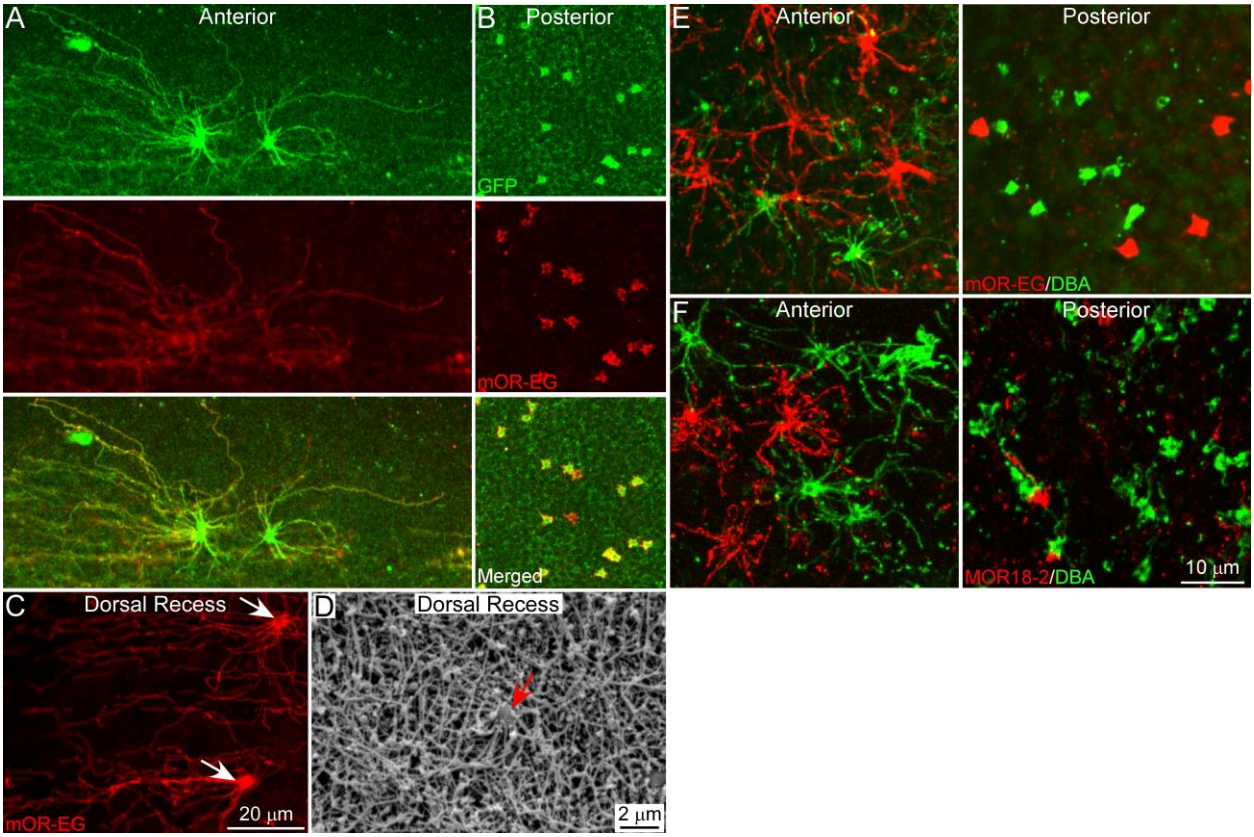


**Figure S2, related to Figure 2. mOR-EG Proteins Are Distributed Throughout the Entire Cilia, and DBA labels OSNs Other Than mOR-EG and MOR18-2 Cells. (A** and **B)** Whole-mount olfactory epithelia from transgenic mOR-EG-IRES-gapEGFP mice (n = 3 animals) were double-stained with antibodies against GFP, which labels the entire ciliary membrane, and mOR-EG, which labels the receptor protein. Co-localization of the mOR-EG and GFP signals indicates that the mOR-EG protein is distributed along the entire cilia. Confocal images were taken from the anterior (**A**) and posterior septum (**B**). Note that a few cells in the posterior region are only stained with the mOR-EG antibody because these cells express one of the endogenous mOR-EG alleles and thus do not express EGFP. (**C** and **D**) mOR-EG cells (**C**) and OSNs under SEM (**D**) from the dorsal recess have visible dendritic knobs (marked by arrows) in regions with lower cell density. Scale bar in (C) applies to (A-C). (**E** and **F**) DBA labels OSNs other than mOR-EG (**E**) and MOR18-2 cells (**F**). Scale bar in (F) applies to (E and F).

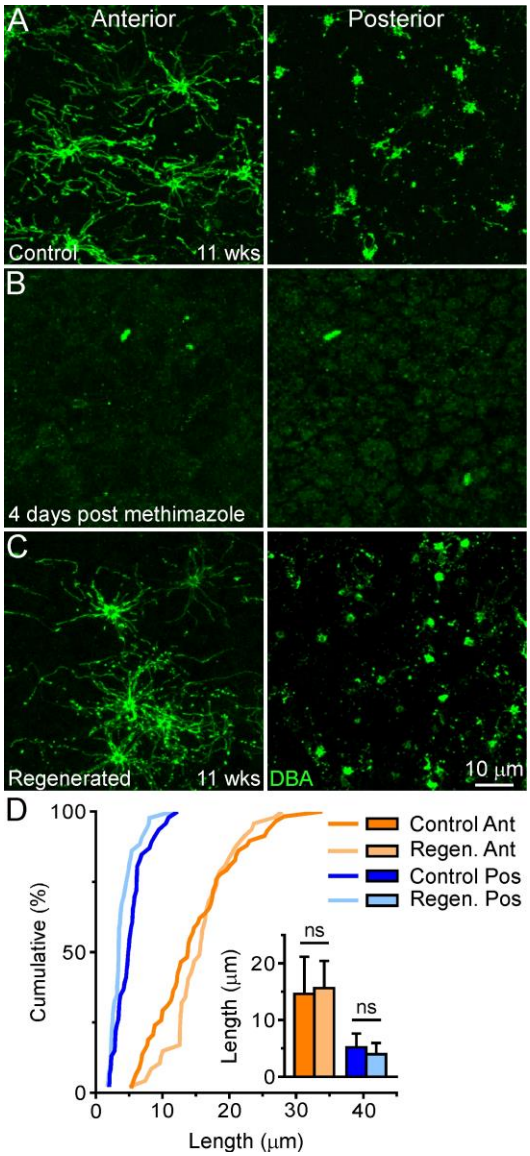


**Figure S3, related to Figure 5. The Cilia Pattern Is Restored Following OSN Regeneration.** (**A-C**) Three-week-old animals were injected with either PBS (**A**) or methimazole (**B** and **C**). Whole-mount olfactory epithelia were stained with DBA four days (B) or eight weeks (A and C) post injection. Scale bar in (C) applies to all images. For simplicity, the cilia lengths from the anterior and posterior septum are compared and quantified. (**D**) Cumulative frequency (%) of cilia length from $DBA^+$ cells in the anterior and posterior regions eight weeks post PBS (control) or methimazole (regenerated) injection. The bar graph shows quantification of cilia length (mean ± SD). Control – Ant: 14.6 ± 6.6 µm, n = 58 cilia; Pos: 5.2 ± 2.4 µm, n = 46 cilia; Regenerated – Ant: 15.6 ± 4.8 µm, n = 47 cilia; Pos: 4.0 ± 2.0 µm, n = 43 cilia; two-way ANOVA, main effect of region: $F = 256.6$, $p < 0.0001$; main effect of treatment: $F = 0.03$, $p = 0.87$; Tukey's multiple comparisons test, ns – not significant.

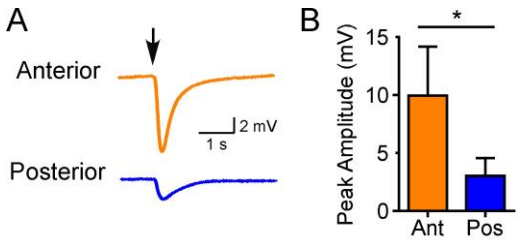


**Figure S4, related to Figure 7. Odorant Stimulation Elicits Larger EOG Signals In the Anterior Versus the Posterior Septum.** (**A**) Representative EOG responses in the anterior and posterior septum (n = 10 animals). The arrow marks the onset of the stimulus (an odorant mixture; see *Supplemental Experimental Procedures*). (**B**) Average peak amplitudes from EOG recordings (mean ± SE). Ant: 10.0 ± 4.1 mV; Pos: 3.0 ± 1.4 mV; paired two-tailed *t* test, * $p < 0.05$.

## Supplemental Tables

| Genotype | Antibody | Cilia Length (μm, mean ± SD ), Cilia Number (n) | | | | | | | | Statistical Test | F | p |
|---|---|---|---|---|---|---|---|---|---|---|---|---|
| | | DR | n | Ant | n | Mid | n | Pos | n | | | |
| C57Bl/6J | mOR-EG | 29.6 ± 11.0 | 99 | 14.7 ± 10.7 | 116 | 8.1 ± 4.6 | 106 | 2.8 ± 2.1 | 126 | One-way ANOVA | 228.2 | < 0.0001 |
| | MOR18-2 | 23.9 ± 4.6 | 89 | 14.9 ± 5.9 | 97 | 7.5 ± 2.9 | 76 | 2.4 ± 1.1 | 115 | One-way ANOVA | 535.7 | < 0.0001 |
| | DBA | 34.6 ± 11.5 | 44 | 22.9 ± 10.1 | 42 | 10.2 ± 5.3 | 47 | 4.7 ± 2.1 | 51 | One-way ANOVA | 131.2 | < 0.0001 |

**Table S1, related to Figures 1 and 2. Cilia length quantification from C57Bl/6J mice.** In all experiments, pairwise comparisons result in significant differences in cilia length between regions.

| Genotype or Condition | Antibody | Cilia Length (μm, mean ± SD ), Cilia Number (n) | | | | | | Statistical Test | F | p |
|---|---|---|---|---|---|---|---|---|---|---|
| | | DR | n | Ant | n | Pos | n | | | |
| $G\gamma13^{+/+}$ | MOR18-2 | 24.4 ± 5.6 | 30 | 15.9 ± 5.6 | 38 | 2.4 ± 1.8 | 50 | Two-way ANOVA[a] | 273.2 | < 0.0001 |
| $G\gamma13^{-/-}$ | MOR18-2 | 28.3 ± 11.6 | 30 | 16.6 ± 8.2 | 47 | 2.8 ± 1.6 | 46 | | | |
| C57Bl/6J Naris Closed | MOR18-2 | 34.6 ± 11.8 | 55 | 28.8 ± 11.4 | 48 | 6.6 ± 3.5 | 50 | One-way ANOVA | 118.4 | < 0.0001 |
| Kir2.1 | MOR18-2 | 24.3 ± 6.6 | 52 | 20.3 ± 8.1 | 50 | 5.0 ± 2.7 | 46 | One-way ANOVA | 124.8 | < 0.0001 |
| C57Bl/6J P0 | DBA | 23.3 ± 5.5 | 35 | 15.3 ± 5.9 | 111 | 3.1 ± 1.8 | 66 | One-way ANOVA | 220.3 | < 0.0001 |
| C57Bl/6J P7 | DBA | 26.3 ± 7.8 | 34 | 16.5 ± 7.4 | 114 | 3.3 ± 1.6 | 110 | One-way ANOVA | 264.5 | < 0.0001 |
| C57Bl/6J P14 | DBA | 32.6 ± 10.3 | 28 | 18.8 ± 8.2 | 97 | 3.0 ± 1.9 | 79 | One-way ANOVA | 224.8 | < 0.0001 |
| $ACIII^{+/+}$ | DBA | 27.0 ± 16.2 | 39 | 14.7 ± 6.2 | 48 | 5.1 ± 2.6 | 43 | Two-way ANOVA | 27.9 (genotype x region interaction) | < 0.0001 |
| $ACIII^{-/-}$ | DBA | 9.3 ± 8.5 | 59 | 8.6 ± 8.1 | 50 | 5.5 ± 4.6 | 52 | | | |

**Table S2, related to Figures 4-6. Cilia length quantification from mice tested under various conditions.** [a] For Gγ13 experiments, there is no interaction between genotype and region. The main effect of region is shown here because the multiple comparisons between genotypes are already included in Figure 4C, which shows no significant differences in cilia length for each region.

## Supplemental Experimental Procedures

***Animals*** All animals were housed in conventional (non-barrier) animal facilities and were 3-8 weeks old, unless otherwise specified. Wild-type C57Bl/6J mice were originally purchased from Jackson Laboratories. The transgenic mouse line mOR-EG-IRES-gapEGFP (IRES = internal ribosome entry site; gapEGFP = GAP-43 N-terminal 20 amino acids fused to enhanced green fluorescent protein) was provided by Dr. Kazushige Touhara's lab [S1]. Olfactory specific $G\gamma13^{-/-}$ animals were generated by crossing mice with a floxed *Gng13* gene, which encodes Gγ13 protein [S2], and $OMP^{Cre}$ mice, in which OMP drives expression of Cre recombinase in mature OSNs [S3]. All $G\gamma13^{-/-}$ animals tested were also $OMP^{Cre/Cre}$ ($G\gamma13^{-/-}/OMP^{Cre/Cre}$), but displayed similar cilia patterns as $G\gamma13^{+/+}/OMP^{Cre/Cre}$ and $G\gamma13^{+/-}/OMP^{Cre/Cre}$ mice. All littermate controls had at least one functional copy of *Gng13* and *Omp*. Kir2.1 mice were obtained by crossing OMP-IRES-tTA mice, in which OMP positive cells also express the transcriptional activator tTA directed by IRES, and $tet_o$-Kir2.1-IRES-taulacZ mice, in which the tTA-responsive promoter $tet_o$ drives the bicistronic expression of the inward rectifying potassium channel Kir2.1 and the marker tau-lacZ [S4]. $ACIII^{-/-}$ mice and $ACIII^{+/+}$ littermate controls were bred from heterozygous $ACIII^{+/-}$ mice [S5]. Although these genetically modified mouse lines were generated using embryos from mixed C57Bl/6J x 129 or C57Bl/6J x DBA2J backgrounds, they were all crossed to C57Bl/6J mice for breeding. For unilateral naris closure, one nostril was briefly cauterized (~1 s) using a cauterizer (Fine Science Tools, Foster City, CA, USA) at postnatal day 3. After 4 weeks, naris closure was confirmed and olfactory epithelia were examined. To induce degeneration of the olfactory epithelium, three-week-old animals were injected intraperitoneally with a single dose (75 mg/kg) of methimazole (Santa Cruz Biotechnology, Santa Cruz, CA, USA) in PBS. Animals were sacrificed at different time points (4 days, 2 weeks, 3 weeks, and 8

weeks after injection) in order to ensure degeneration of the epithelium and monitor recovery over time [S6]. All procedures were approved by the Institutional Animal Care and Use Committee.

***Immunohistochemistry*** Mice were anesthetized by ketamine/xylazine injection (200 and 20 mg/kg body weight) and then decapitated. Newborn pups were anesthetized by hypothermia. Partially dissected heads were fixed in 4% paraformaldehyde (Sigma-Aldrich, St. Louis, MO, USA) in 1X phosphate buffered saline (PBS) overnight at 4°C and washed 3x for 5 min in PBS the next day. The nasal septum or turbinates were dissected out *en bloc*, washed 3x in PBS, and blocked for 1–2 h at room temperature (RT) in 3% bovine serum albumin (Jackson ImmunoResearch Laboratories, West Grove, PA, USA) in PBS. Incubation with primary antibodies in blocking solution was performed overnight at 4°C. The primary antibodies include guinea pig anti-mOR-EG (1:250), rabbit anti-GFP (1:1000; A11122, Life Technologies, Carlsbad, CA, USA), rabbit anti-MOR18-2 (1:400), biotinylated *Dolichos biflorus* agglutinin (DBA) (5 mg/mL, 1:300 working dilution; B-1035, Vector Laboratories, Burlingame, CA, USA), and rabbit anti-MOR28 (1:6000). Tissues were washed 3x with 0.3% Triton-X-100 (Roche Diagnostics, Indianapolis, IN, USA) in PBS (TPBS), and then incubated for 1 h at RT with secondary antibodies conjugated to Alexa Fluors (Life Technologies). The secondary antibodies include goat anti-guinea pig IgG (1:400; A11073 and A11075), donkey anti-rabbit IgG (1:400, A21206 and A10042), and streptavidin conjugate (1:1000; S32354 and S11226). Tissues were then washed 2x for 5 min in TPBS and 1x for 5 min in PBS. To facilitate comparison among different preparations, olfactory epithelia along the septum were marked with a small quantity of colored tissue dye (1163, Bradley Products, Inc., Bloomington, MN, USA) at

a fixed location, defined as the most dorsal point where the nasal septal cartilage meets the ethmoid bone (see Figure 1A). Olfactory mucosa were peeled away from the underlying bone and mounted in Vectashield mounting medium (Vector Laboratories). Images (z-step = 1 μm) were taken under a Leica TCS SP5 II confocal microscope (Leica Microsystems, Buffalo Grove, IL, USA) with a 40x oil objective. Cilia were traced using Leica LAS AF Lite software.

***Regional Subdivisions and Cilia Quantification*** The olfactory epithelium along the septum was divided into four regions (DR, Ant, Mid, and Pos) based on the cilia morphology characteristically found in each area. During imaging, regional boundaries were measured with respect to their distance from a fixed location, which was marked with dye prior to mounting the tissues (see *Immunohistochemistry* and Figure 1A). The center of the Ant, Mid, and Pos regions is approximately 1.5 mm anterior, 0.5 mm ventral; 1 mm posterior, 0.5 mm ventral; and 2 mm posterior, 1.5 mm ventral to the dye mark, respectively. The DR can be identified without reference to the dye mark since it is not attached to the septum and easily recognized by gross anatomy. The Mid and Pos regions (i.e., where cells with shorter cilia are observed) are typically the smallest areas, while the DR and Ant regions (i.e., where cells with longer cilia are observed) are the largest areas. Cilia from the Mid and Pos regions are mostly non-overlapping and can be unambiguously measured. In the DR and Ant, many cilia are difficult to trace from the origin to the end, but some cells stand alone and allow accurate measurement of their cilia length (see Figure S2). Because all animals under the same condition showed similar cilia length patterns, we sampled cilia from representative images for each condition.

***Scanning Electron Microscopy*** Samples for SEM were dissected and fixed in 2.5% glutaraldehyde and 2.0% paraformaldehyde in 0.1 M cacodylate buffer (pH 7.4) overnight at 4ºC. After several buffer washes, samples were post-fixed in 2.0% osmium tetroxide for 1 hr, washed again in buffer, and dehydrated in a graded ethanol series. Samples were treated several times with hexamethyldisilazane (HMDS) and then allowed to air dry prior to mounting and sputter coating with gold/palladium. SEM examinations were made, and images were taken in a Philips XL20 scanning electron microscope.

***qRT-PCR*** The DR, Ant, and Pos regions of the olfactory epithelia from three wild-type littermates were dissected in ice-cold RNAse-free 1X PBS and snap frozen on dry ice. The left and right epithelia of each animal were pooled; biological replicates remained separate. RNA was purified using the RNAeasy Mini Kit (Qiagen, Valencia, CA, USA), including a DNAse I digestion step (Qiagen). Total RNA was reverse transcribed using SuperScript III First Strand Synthesis System (Invitrogen, Carlsbad, CA, USA). Quantitative PCR was performed using SYBR Green PCR Master Mix (Applied Biosystems, Carlsbad, CA, USA) and 1 ng cDNA (i.e., 1 ng RNA converted 1:1 to cDNA) per reaction. Primers were designed to span an exon-exon junction whenever possible to prevent amplification of genomic DNA. *Adcy3* forward – CCCAGAGATGGAAACACGCT; *Adcy3* reverse – TTTGTCATCAGCCAGGGGTC; *Omp* primers were used as reported previously [S2]. All biological replicates were run in triplicate. *Adcy3* expression was analyzed using the comparative cycle threshold ($C_T$) ($\Delta\Delta$ $C_T$) method and was normalized to *Omp* expression. Fold change is reported as mean ± standard deviation (SD) across all three animals.

***Cilia Length Heatmaps*** Cilia length heatmaps were generated by averaging the cilia lengths of mOR-EG cells from over 60 evenly distributed locations (each at 400 x 400 $\mu m^2$) throughout the dorsal recess, septum, and endoturbinates and filling in the non-measured areas by linear interpolation function.

***Computational Fluid Dynamics Model and Correlation Analysis*** A six-week-old B6129PF2/J mouse was euthanized with $CO_2$ and decapitated. The head was fixed in 4% paraformaldehyde overnight at 4°C. The specimen was then wrapped and sealed with Parafilm before being placed in a Viva CT 40 microCT scanner (Scanco USA, Inc.). A total of 3300 images, 2048 x 2048 pixels each and with an isotropic resolution of 10.5 μm per pixel, were obtained with a bulb setting of 70 kv and 114 μA. A 3D median filter with a mask of 5 x 5 x 7 pixels was applied to remove image noise and preserve the edge between the airway and mucosa.

An anatomically accurate 3D nasal model was constructed based on the segmentation of the microCT images using three different types of software: AMIRA (Visualization Sciences Group, Burlington, MA, USA), ICEM, and FLUENT (both from Ansys, Inc., Canonsburg, PA, USA) with a total of $1.8\times10^7$ cells in order to completely resolve the airspace and the boundary layer where odorant molecules become trapped [S7, S8]. The steady state odorant deposition through airflow and mucosal uptake of vaporized eugenol was simulated based on the calculated airflow field and estimated physicochemical properties [S9]. In short, odorant concentration at the boundary of the air-mucus interface satisfied: $\frac{\partial C'}{\partial y'} + KC' = 0$ with $K = \frac{d_{in} D_m}{D_a \beta H_m}$, where $d_{in}$ is the hydraulic diameter (4 × area / perimeter) of the nostril, $D_m$ is the eugenol diffusion coefficient in water ($6.47 \times 10^{-6}$ $cm^2/s$), β is the air/water partition coefficient (defined by the

ratio of odorant concentration in the air phase to the concentration in mucus, $1.95 \times 10^{-6}$), $H_m$ is the thickness of the mucosal layer and also the path length that odorant molecules need to diffuse through (30 μm), and $D_a$ represents the diffusivity of odorant molecules through air (0.062 $cm^2/s$).

The potential correlation was evaluated by plotting odorant absorption values from 55 evenly distributed locations throughout the dorsal zone versus the corresponding average cilia length measurement from each location (see Figure 3C). The number of locations in each region is approximately proportional to its surface area (n = 28 from dorsal recess, 17 from the septum, and 10 from the endoturbinates). Analysis was performed using the Pearson correlation calculation.

***Patch Clamp and EOG Recordings*** Intact epithelia were prepared as in our published procedures [S10, S11]. Mice were deeply anesthetized by ketamine injection and then decapitated. The head was immediately placed into ice-cold Ringer's solution which contained (in mM): 124 NaCl, 3 KCl, 1.3 $MgSO_4$, 2 $CaCl_2$, 26 $NaHCO_3$, 1.25 $NaH_2PO_4$, and 15 glucose (pH 7.6 and 305 mOsm); the pH was kept at 7.4 after bubbling with 95% $O_2$ and 5% $CO_2$. The nose was dissected out *en bloc*, and the olfactory epithelium attached to the nasal septum and the dorsal recess was removed and kept in oxygenated Ringer's. Before use, the entire epithelium was peeled away from the underlying bone and transferred to a recording chamber with the mucus layer facing up. Oxygenated Ringer's was continuously perfused at 25 ± 2ºC.

The dendritic knobs of OSNs were visualized through an upright microscope (Olympus BX61WI) with a cooled CCD camera (SensiCam QE, PCO) and a 40x water-immersion objective. An extra 4x magnification was achieved by an accessory lens in the light path. GFP-

tagged cells were visualized under fluorescent illumination. Superimposition of the fluorescent and bright field images allowed identification of fluorescent cells under bright field, which directed the recording pipettes [S10]. Electrophysiological recordings were controlled by an EPC-9 amplifier combined with Pulse software (HEKA Electronic, Germany). Perforated patch-clamp was performed on the dendritic knobs by including 260 μM nystatin in the recording pipette, which was filled with the following solution (in mM): KCl 70, KOH 53, methanesulfonic acid 30, EGTA 5.0, HEPES 10, sucrose 70; pH 7.2 (KOH) and 310 mOsm. The junction potential was ~ 9 mV and corrected off-line.

EOG recordings were performed as previously described [S5, S12]. Mice (8 to 12 weeks old) were sacrificed by decapitation, and the nose was dissected out *en bloc*. Odorized air was produced by blowing nitrogen (2.4 L/min at 22°C) through a horizontal glass cylinder filled halfway with an odorant mixture comprised of acetophenone, butyric acid, R-(−)-carvone, citralva, ethyl vanillin, eugenol, 1-heptanol, 2-heptanone, 3-heptanone, R-(+)-limonene, S-(−)-limonene, and octanal, each at 100 μM in Ringer's solution containing ≤ 0.2% dimethyl sulfoxide (DMSO). Air puffs were delivered locally to either the anterior or posterior regions of the exposed nasal septum for 200 ms using an automated four-way slider valve (P/N: 330224S303, ASCO) controlled by a computer via an S48 Stimulator (Glass Technologies). The tip of the puff application tube was 1.5–2.0 cm away from the surface of the epithelium and pointed directly at the recording site.

The EOG field potential was detected with a glass microelectrode filled with agar and Ringer's solution. EOG signals were amplified with a CyberAmp 320, digitized at 1–10 kHz using Digidata 1332A and MiniDigi 1A processors, and acquired with pClamp 10.3 and

Axoscope 10 software (Molecular Devices). Exclusion of artifacts during EOG recordings and data analyses was performed as previously described [S12].

**Supplemental References**


S1. Oka, Y., Katada, S., Omura, M., Suwa, M., Yoshihara, Y., and Touhara, K. (2006). Odorant receptor map in the mouse olfactory bulb: in vivo sensitivity and specificity of receptor-defined glomeruli. Neuron *52*, 857-869.

S2. Li, F., Ponissery-Saidu, S., Yee, K.K., Wang, H., Chen, M.L., Iguchi, N., Zhang, G., Jiang, P., Reisert, J., and Huang, L. (2013). Heterotrimeric G protein subunit Ggamma13 is critical to olfaction. J. Neurosci. *33*, 7975-7984.

S3. Li, J., Ishii, T., Feinstein, P., and Mombaerts, P. (2004). Odorant receptor gene choice is reset by nuclear transfer from mouse olfactory sensory neurons. Nature *428*, 393-399.

S4. Yu, C.R., Power, J., Barnea, G., O'Donnell, S., Brown, H.E., Osborne, J., Axel, R., and Gogos, J.A. (2004). Spontaneous neural activity is required for the establishment and maintenance of the olfactory sensory map. Neuron *42*, 553-566.

S5. Wong, S.T., Trinh, K., Hacker, B., Chan, G.C., Lowe, G., Gaggar, A., Xia, Z., Gold, G.H., and Storm, D.R. (2000). Disruption of the type III adenylyl cyclase gene leads to peripheral and behavioral anosmia in transgenic mice. Neuron *27*, 487-497.

S6. Suzukawa, K., Kondo, K., Kanaya, K., Sakamoto, T., Watanabe, K., Ushio, M., Kaga, K., and Yamasoba, T. (2011). Age-related changes of the regeneration mode in the mouse peripheral olfactory system following olfactotoxic drug methimazole-induced damage. J. Comp. Neurol. *519*, 2154-2174.

S7. Zhao, K., Dalton, P., Yang, G.C., and Scherer, P.W. (2006). Numerical modeling of turbulent and laminar airflow and odorant transport during sniffing in the human and rat nose. Chem. Senses *31*, 107-118.

S8. Jiang, J., and Zhao, K. (2010). Airflow and nanoparticle deposition in rat nose under various breathing and sniffing conditions: a computational evaluation of the unsteady effect. J. Aerosol. Sci. *41*, 1030-1043.

S9. Kurtz, D.B., Zhao, K., Hornung, D.E., and Scherer, P. (2004). Experimental and numerical determination of odorant solubility in nasal and olfactory mucosa. Chem. Senses *29*, 763-773.

S10. Grosmaitre, X., Vassalli, A., Mombaerts, P., Shepherd, G.M., and Ma, M. (2006). Odorant responses of olfactory sensory neurons expressing the odorant receptor MOR23: a patch clamp analysis in gene-targeted mice. Proc. Natl. Acad. Sci. USA *103*, 1970-1975.

S11. Ma, M., Chen, W.R., and Shepherd, G.M. (1999). Electrophysiological characterization of rat and mouse olfactory receptor neurons from an intact epithelial preparation. J. Neurosci. Methods *92*, 31-40.

S12. Chen, X., Xia, Z., and Storm, D.R. (2012). Stimulation of electro-olfactogram responses in the main olfactory epithelia by airflow depends on the type 3 adenylyl cyclase. J. Neurosci. *32*, 15769-15778.